Growth of WC–Cr–N and WC–Al–N coatings in a RF-magnetron sputtering process

Andrei V. Stanishevsky [a,*], Michael J. Walock [a,b], Yujiao Zou [a], Luc Imhoff [c], Amel Zairi [b,d], Corinne Nouveau [b]

[a] University of Alabama at Birmingham, Department of Physics, 1300 University Boulevard, CH310, Birmingham, AL 35294-1170, USA
[b] Laboratoire Bourguignon des Matériaux et Procédés, CER Arts et Métiers ParisTech of Cluny, F-71250 Cluny, France
[c] Institut Carnot de Bourgogne, UMR 5209 CNRS, Université de Bourgogne, 9 Avenue Alain Savary, BP 47870, 21078 Dijon Cedex, France
[d] Laboratoire de Mécanique, Matériaux et Procédés, Ecole Supérieure des Sciences et Techniques de Tunis, Tunis, Tunisia

ARTICLE INFO

Article history:
Received 11 October 2011
Received in revised form
31 March 2012
Accepted 22 May 2012

Keywords:
Magnetron sputtering
Thin films
Tungsten carbide
Nitrides
Coatings

ABSTRACT

Tungsten carbide-based coatings have been used in a wide variety of industrial applications such as high speed cutting tools, extrusion dies, drills, aerospace industries, and more. A few reports on ternary and quaternary coatings of WC with other elements indicate good prospects for these material systems. The present study focuses on the formation of quaternary WC–Cr–N and WC–Al–N coatings during the simultaneous reactive RF-magnetron sputtering of tungsten carbide and Al or Cr targets in an argon/nitrogen gas mixture. The resulting coatings, with thicknesses of 3.5 μm–8.2 μm, were characterized by using several analytical techniques including X-ray diffraction, SEM/EDS, AFM, and X-ray photoelectron spectroscopy. WC–Cr–N and WC–Al–N coatings with high levels of tungsten (i.e. more than 50 at.% of the total metal content) demonstrated dense microstructure. Coatings with lower tungsten content formed columnar grain microstructure, with different surface morphologies depending on the process parameters. It was proposed that crystalline tungsten carbide (with partial N-substitution of C atoms) and chromium (or aluminum) nitride phases coexist in the coatings when the amount of tungsten was greater than 50 at.% of the total metal content; while at lower tungsten content, the dominating crystalline phase is either W-doped CrN_{1-y} or AlN_{1-y} solid solution, with WC_{1-x} and small amounts of free sp^2-bonded carbon present as X-ray amorphous phases.

1. Introduction

The development of plasma-assisted vacuum coating processes, such as physical vapor deposition (PVD), allowed the fabrication of a multitude of metal nitride, carbide, and oxide coatings that can significantly improve the performance and durability of precision components. The technological challenges in surface engineering over the last decade have put new special requirements on such coatings with, in many cases, nanolayered ("nanolaminate") or nanocomposite structures to further extend the coatings' functionality and the performance of coated parts [1,2].

These coatings can exhibit unique property combinations, e.g., super-hardness (>40 GPa) combined with high toughness and thermal stability [3–6]. Such combinations of useful properties cannot be reached in binary compounds like metal carbides or nitrides. These property combinations are realized by a functional nanostructure, mainly achieved in ternary and/or quaternary systems. Some examples of such coatings include Ti–Al–N, Ti–Si–C–N, Si–B–C–N, Ti–B–N–C, Ti–N–O–C [7–11], to name just a few. Although there are fewer publications on hard quaternary nanocomposite coating systems when compared with ternary, it has been shown that quaternary systems offer more flexibility for obtaining the desired combination of properties (e.g., a compromise of high hardness and toughness) by optimizing the ratio and arrangement of amorphous and nanocrystalline phases. For example, the addition of carbon into hard Ti–Si–N or Co–Mo–N ternary systems led to quaternary nanocomposite coatings with further increased hardness and reduced coefficient of friction [12,13].

Relatively few reports can be found on ternary and quaternary coatings based on tungsten, although those reports have demonstrated good prospects for these material systems [14,15]. Tungsten carbide is of great interest due to its high melting point, superior hardness among other binary carbides and nitrides, low friction coefficient, considerable elastic modulus, small thermal expansion

coefficient, and high thermal resistance. WC-based materials have been used in a wide variety of industrial applications in high-temperature tools and devices: high-speed cutting tools, extrusion dies, drills, aerospace industries, etc. [16,17]. This determined the search for new WC-based materials with non-trivial combinations of operating characteristics like W_2AlC and $WAlC_2$ [18]. It has been suggested that adding Al into the WC lattice to form a solid solution can enhance the bending strength of the material [19]. Several nitride and carbide coating systems based on W–Cr and W–Al show strong promise for achieving the excellence as hard and tough thermally stable tribological coatings in several technological applications [20–22]. $CrWN_2$ layered ternary compounds with potentially interesting properties have also been described [23]. W–Al–N films show exceptional corrosion resistance and reduced tendency of tungsten to oxidize at elevated temperatures [24]. Ternary $Cr_{0.6}W_{0.4}N$ films were found to exhibit a fine-grained dense morphology without apparent superstructure, low friction and high hardness [25]. CrN/WN superlattices have been shown to noticeably improve hardness over single layer CrN or WN films [26].

The present study focuses on the formation of quaternary WC–Cr–N and WC–Al–N coatings during the simultaneous reactive RF-magnetron sputtering of tungsten carbide and Al or Cr target in argon/nitrogen gas mixture.

2. Experimental

2.1. Coating deposition

Both WC–Cr–N and WC–Al–N coatings were prepared by reactive RF magnetron sputtering in a modified commercial system (Nordiko 3500). This system is equipped with two 4 in diameter magnetron sputtering guns powered by individual RF generators operating at 13.56 MHz. The guns are arranged confocally, at ±45° with respect to the sample normal. Substrate to target distance was 8 cm. The targets were Cr (or Al) (Neyco, 99.95%) and WC (Neyco, 99.5%) and the base pressure was 6×10^{-5} Pa. For improved adhesion, the silicon (110) substrates were cleaned and a 50 nm Cr–WC or Al–WC buffer layer was deposited to improve adhesion. The substrates were first cleaned chemically and then in a 12 kV DC glow discharge pulsed (25 μs on/50 ms off) for 5 min at an Ar pressure of 2 Pa. The deposition parameters for the WC–Cr–N and WC–Al–N coatings are summarized in Table 1. The target bias voltages were systematically varied to obtain different (Cr or Al): W ratios. For the WC–Cr–N coatings, the Ar/N_2 ratio was fixed at 60/40. This is within the "compound" range of the reactive sputtering regime. For the WC–Al–N coatings, the nitrogen partial pressure was reduced, resulting in an Ar/N_2 ratio of 80/20. This falls within the "metallic" reactive sputtering regime. This was primarily chosen due to significant Al target poisoning and plasma coupling between the WC and Al targets. This led to unstable plasma at higher nitrogen content. Substrates were grounded and the substrate temperature was in the range 170 °C–200 °C in these experiments.

Table 1
Summary of deposition conditions for WC–Cr–N and WC–Al–N coatings.

Targeted Cr:W ratio	Gas		Target				Growth rate, nm/min
	Total Pressure	Ar/N_2 ratio	WC		Cr		
			Bias	Power	Bias	Power	
1:1	1 Pa	60/40	−600 V	200 W	−300 V	100 W	7.8
2:1	1 Pa	60/40	−600 V	225 W	−600 V	500 W	12.3
3:1	1 Pa	60/40	−600 V	200 W	−900 V	500 W	16.4
4:1	1 Pa	60/40	−450 V	150 W	−900 V	500 W	16.0
Targeted Al:W ratio	Gas		Target				Growth rate, nm/min
	Total	Ar/N_2	WC		Al		
			Bias	Power	Bias	Power	
1:1	1 Pa	80/20	−800 V	900 W	−800 V	100 W	18.2
2:1	1 Pa	80/20	−800 V	850 W	−400 V	150 W	15.8
3:1	1 Pa	80/20	−275 V	60 W	−800 V	600 W	16.0
4:1	1 Pa	80/20	−200 V	50 W	−800 V	700 W	10.9

2.2. Characterization methods

The surface morphology of the coatings was investigated with field-emission scanning electron microscopy (FE-SEM, JEOL JSM 6400F, also used for imaging the cross-sections of the coatings) and atomic force microscopy (AFM, Veeco Topometrix Explorer). SEM imaging was done in secondary electron mode, with an accelerating voltage of 20 kV, and a chamber pressure of 1×10^{-4} Pa. Chemical composition was determined by electron dispersive spectroscopy (EDS, Oxford INCA x-act). During EDS, the accelerating voltage was 5 kV with an integration time of 100 s. Surface roughness characteristics were explored using AFM in contact mode, using v-shaped, high resonance frequency SiN cantilevers with a pyramidal tip of 50 nm radius and a force constant of 0.032 N/m. The crystalline phase composition was investigated by thin-film X-ray diffraction (XRD, Philips X'pert MPD) with a Cu Kα tube ($\lambda = 0.15406$ nm) operating at 45 kV and 40 mA. The detector was scanned between 20° and 70°, with a constant take off angle of 5°. The peak parameters were determined with the CMPR program [27], and the experimental diffraction patterns were compared with the ICDD powder diffraction file (PDF) database [28]. The crystallite size was estimated using the Scherrer equation.

A PHI 5000 Versaprobe imaging X-ray photoelectron spectrometer (XPS), operating a monochromatic, focused Al Kα X-ray source ($E = 1486.6$ eV) at 25 W with a 100 μm spot size, was used to determine the chemical bonding in the coatings. All samples were grounded. Charge neutralization was provided by a cold cathode electron flood gun and low-energy Ar-ions. All measurements were taken at room temperature and at a pressure of 2×10^{-6} Pa (the system base pressure is 5×10^{-8} Pa). Surface sputtering was not used in these experiments to avoid the possibility of the change in the chemical bonding state associated with ion-induced damage. Multipak v9.0 software was used to analyze the resulting spectra.

3. Results and discussion

All WC–Cr–N and WC–Al–N coatings prepared under the conditions given in Table 1 were uniform, smooth, and well adherent to the substrates. According to the XRD data (Fig. 1 and Fig. 2), all coatings were nanocrystalline. However, the size of crystallites for Cr:W or Al:W with a targeted ratio of 1:1 cannot be reliably identified. The XRD patterns of both WC–Cr–N and WC–Al–N coatings in this case show one broad asymmetric peak that can be an overlap of the reflections from several WC*x* crystalline phases, as well as CrN or AlN, depending on the process. For comparison, the sputtering of WC target alone in Ar/N_2 mixture results in similar single broad peak XRD pattern, while the sputtering of WC target in argon only leads to a typical XRD pattern of nanocrystalline WC_{1-x} (PDF 00-020-1316) (spectra no shown here).

When the ratio of Cr:W or Al:W in the coatings increases, well-defined XRD patterns appear. The threshold composition at which this change in the phase composition occurs was not determined in these experiments. For samples with Cr:W or Al:W targeted ratios of 2:1 or larger, the average size of crystallites is in the 9 nm–13 nm range.

A cubic phase was suggested in WC–Cr–N coatings, where the (111) and (200) peak positions are between those in cubic WC_{1-x}

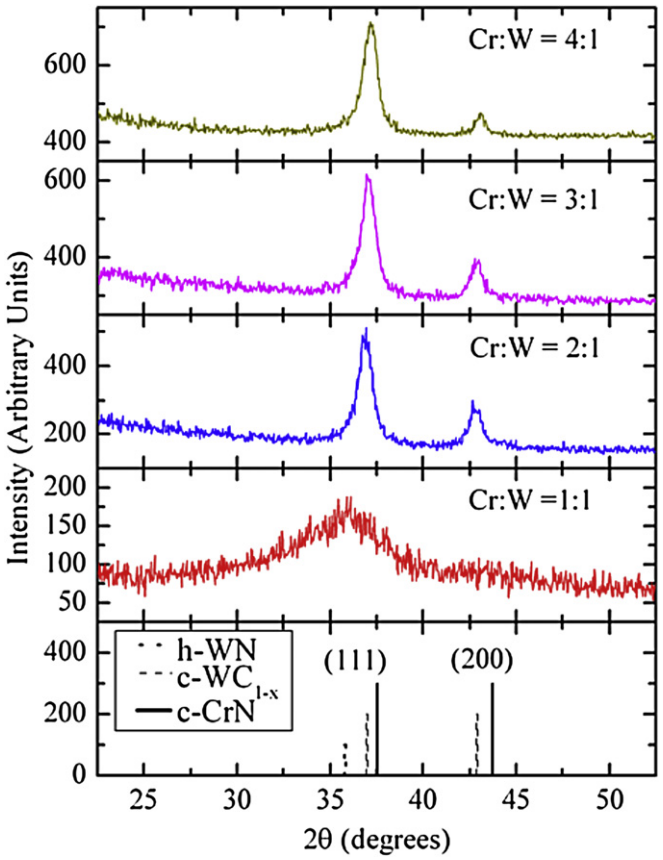

Fig. 1. X-ray diffraction patterns of WC–Cr–N samples with Cr:W targeted ratios of 1:1, 2:1, 3:1, and 4:1. The dotted line represents the position of h-WN peaks, the dashed line is c-WC_{1-x}, and the solid line is CrN.

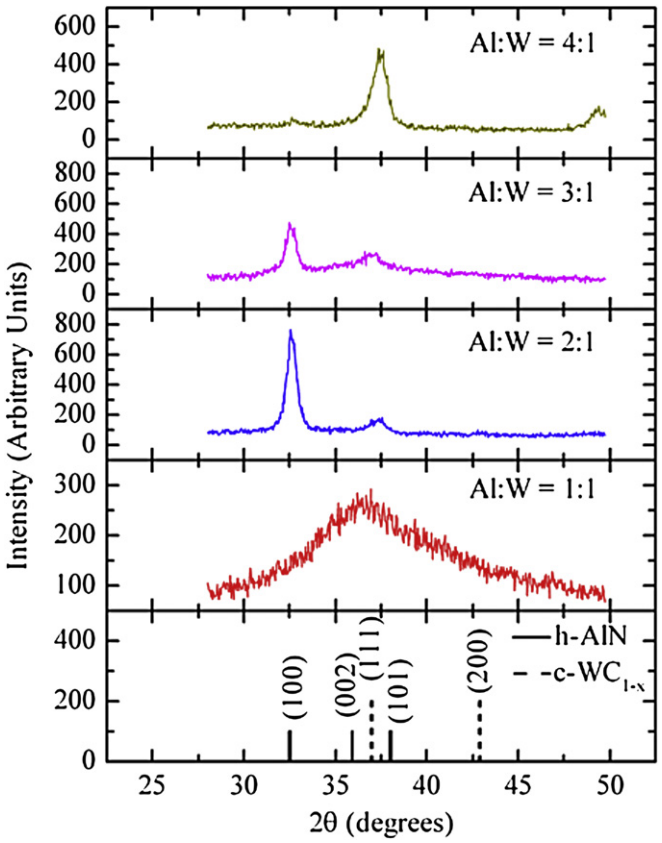

Fig. 2. X-ray diffraction patterns of WC–Al–N samples with Al:W targeted ratios of 1:1, 2:1, 3:1, and 4:1. The solid line represents the position of h-AlN peaks, and the dashed line is c-WC_{1-x}.

and CrN phases. The positions of both (111) and (200) peaks in WC–Cr–N shift towards those of CrN as the Cr:W ratio increases. For example, (111) peak is located at 36.9° in the sample with Cr:W = 2:1, 37.06° when Cr:W = 3:1, and 37.16° when Cr:W = 4:1.

The XRD patterns of WC–Al–N coatings with Al:W ratio of 2:1 or higher are close to hexagonal AlN phase (Fig. 2). Furthermore, WC–Al–N coatings show significant changes in the preferred crystalline orientation with the increasing content of aluminum. The preferred orientation changes from (100) to (101) with a latter peak being shifted to a lower angle from that of h-AlN. One possible reason for the change in preferred orientation is the effects of the increased sputtering yield and the energy of the sputtered species that influences the nucleation and subsequent film growth as discussed in previous studies [29,30]. Indeed, to change the Al:W ratio, the rf-power on the aluminum target was varied from 100 W to 700 W (Table 1), which results in an increase in the both the energy of sputtered particles and the sputtering yield [31]. With these increases, the adatom mobility is limited, leading to crystalline orientations with higher formation energies, such as (101) [29]. In the case of WC–Cr–N coatings, the rf-power on the Cr-target was constant (Table 1), and little changes were observed in the XRD patterns of the coatings with Cr:W ratios 2:1 and higher.

SEM investigation revealed a strong dependence on the deposition parameters of both the WC–Cr–N and WC–Al–N coatings' microarchitecture and their surface morphology. Fig. 3 presents SEM images of the cross-sections and surfaces of WC–Cr–N coating samples. It can be seen that the WC–Cr–N sample with Cr:W targeted ratio of 1:1 is dense and nearly featureless. Similar result was found for the WC–Al–N sample with Al:W targeted ratio of 1:1 (Fig. 4). SEM images of the cross-sections of all other WC–Cr–N and WC–Al–N with a higher concentration of Cr and Al, respectively, indicate the formation of the columnar grain structure. The surface morphology of these samples showed drastic variations from sample to sample. The increase in Cr content in WC–Cr–N coatings leads to gradually sharper surface features. On the other hand, the changes in the surface morphology of WC–Al–N do not follow a specific trend. The change in the preferred crystalline orientation with the increasing Al content can be one of the influencing factors in this case [29]. However, the surface morphology in Fig. 4(d) ((101) preferred orientation) has been observed in [29] for AlN films with (100) preferred orientation. The coatings in Fig. 4 (b) and (c) have the same (100) orientation but their surface morphology is very different as well. Therefore, other factors such as the presence of WC-component, film growth rate (defects flow), secondary nucleation during the growth, and stress, have to be considered in unison to explain, in part, the formation of surface morphology of quaternary coatings [32–34]. For example, the growth rate of WC–Cr–N and WC–Al–N in present study ranged from 7.8 nm/min to 16.4 nm/min (see Table 1 for the growth rates of specific samples). One can find that significant changes in the surface morphology of the coatings were observed even for nearly the same growth rate. Thus, the growth rate is hardly a determining factor in the development of the observed surface features.

A concurrent AFM study of the WC–Cr–N and WC–Al–N coatings indicated a trend of increasing surface roughness at higher Cr:W or Al:W ratios. Fig. 5 presents the graphs of the Ra and RMS roughness parameters as functions of the Cr or Al content in the coatings. The roughness of all coatings was found in sub-10 nm

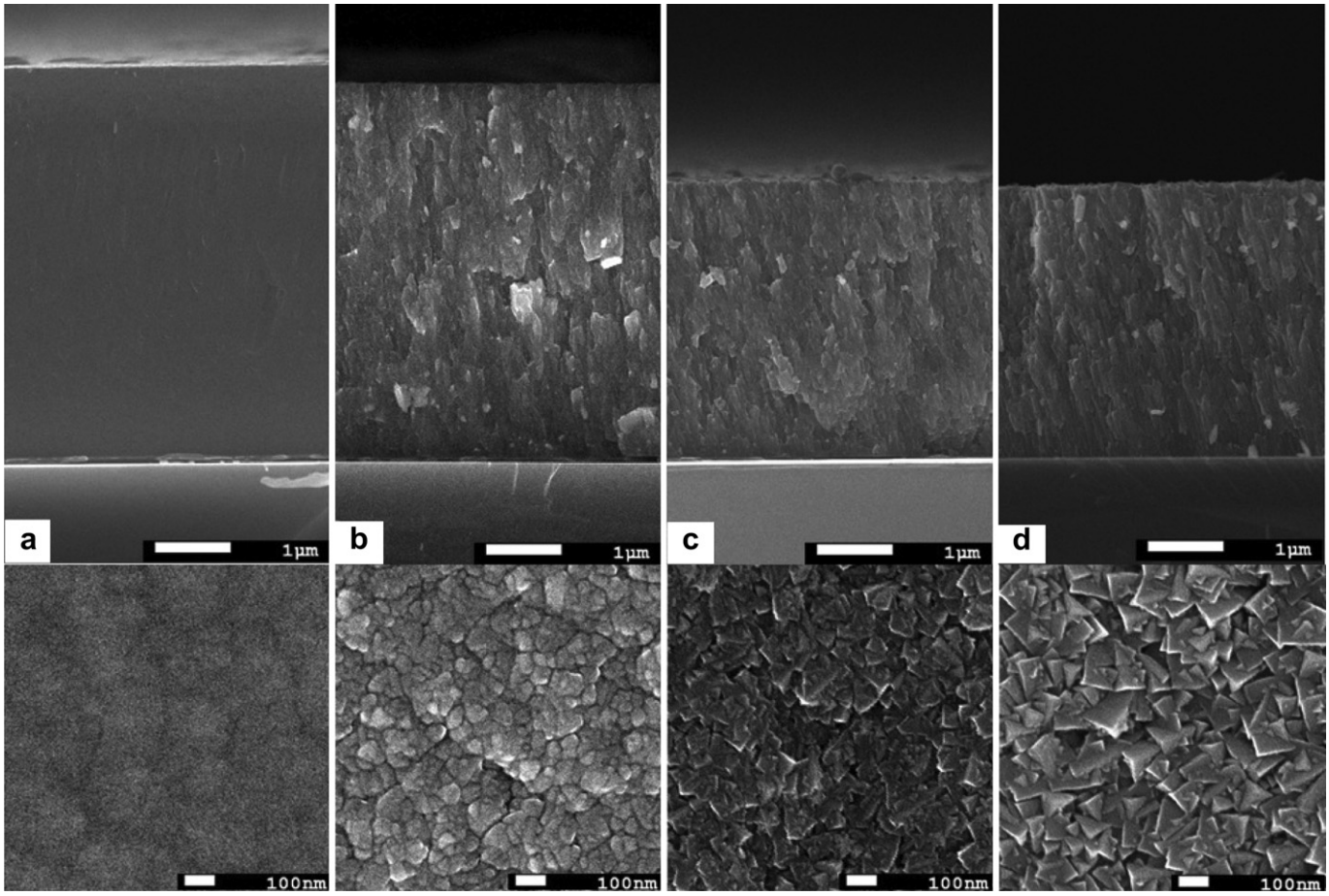

Fig. 3. Secondary electron images of the cross-sections (top row) and surface (bottom row) of WC–Cr–N coatings with Cr:W targeted ratios of (a) 1:1, (b) 2:1, (c) 3:1, and (d) 4:1.

range. The roughness of the coatings with Cr:W or Al:W targeted ratios 1:1 was only slightly higher than that of binary WC_{1-x} prepared under the same sputtering conditions. For other ratios, WC–Cr–N coatings were noticeably rougher than WC–Al–N coatings.

The results of EDS and XPS studies draw a more detailed picture of the phase and chemical compositions of the prepared quaternary coating systems. Table 2 relates the targeted ratios used above to the actual data on the chemical composition of WC–Cr–N and WC–Al–N coatings, as measured by EDS. The EDS and XPS composition data match each other fairly well for the exception of oxygen concentration, which was higher in XPS study. This difference may be due to the effective probing depths of EDS versus XPS. XPS is a surface-sensitive technique, with a probing depth of only a few nanometers. However, EDS (using an accelerating voltage of 5 kV in coatings containing a high-density material) has a significantly larger probing depth of a few hundred nanometers. As such, EDS is less susceptible to "errors" due to significant surface oxidation. Additionally, it should be noted, that while high deposition rates would decrease the nitrogen content of the coatings, this trend is not observed.

Summarizing the XPS results for WC–Cr–N, no noticeable changes in the position of Cr2p electron binding energy level (573 eV, not shown) were noted. The N1s energy level was recorded at 395.8 eV in the coating with Cr:W = 1:1, and it was at 395.6 eV in other samples. This could indicate that chromium is mostly present in a form of chromium nitride in all WC–Cr–N coatings. The W4f energy level gradually shifted from 30 eV to 29.64 eV with the increase of Cr content. This could be due to partial dissolution of Cr in carbon-deficient WC_{1-x} [35]. The only significant changes were observed in the energy states of carbon C1s electron. The C1s energy level spectrum for the sample with Cr:W = 1:1 can be fitted with a distinct peak at 281.5 eV and two very small peaks at 283 eV and 284.3 eV (Fig. 6). The C1s energy level spectrum for the samples with higher Cr:W ratios shows two distinct peaks at 281.5 eV and 283 eV with a small peak at 284.3 eV. It has been suggested that such trends in XPS spectra of WC–Cr–N are connected with the formation of W–C and W–C–W bonds in carbon-deficient WC_{1-x}, and the presence of free carbon in sp^2-bonding state (peak at 284.3 eV). The presence of free sp^2-bonded carbon has been confirmed by the presence of broad scattering around 1600 cm^{-1} in the Raman spectra of these coatings. These results show that W–C and Cr–N are the dominating chemical bonds in WC–Cr–N. It is hypothesized that crystalline tungsten carbide (with partial N-substitution of C atoms) and chromium nitride phases can coexist in the coatings with Cr:W = 1:1 and lower, while at higher Cr:W ratios a major crystalline phase is W-doped CrN_{1-y} solid solution [14], with WC_{1-x} and small amounts of free sp^2-bonded carbon as X-ray amorphous phases.

The W4f, N1s, and Al2p electron energy levels located at 30.1 eV, 395.6 eV, and 72.3 eV, respectively, in WC–Al–N coatings with Al:W = 1:1, shift all by 0.7 eV to higher binding energies when the Al:W ratio reaches 3:1 and higher. This may be associated with uncompensated surface charge in these coatings composed mainly of an electrically insolating AlN phase. The carbon C1s level in the Al:W = 1:1 coating splits in the same three peaks (281.5 eV, 283 eV,

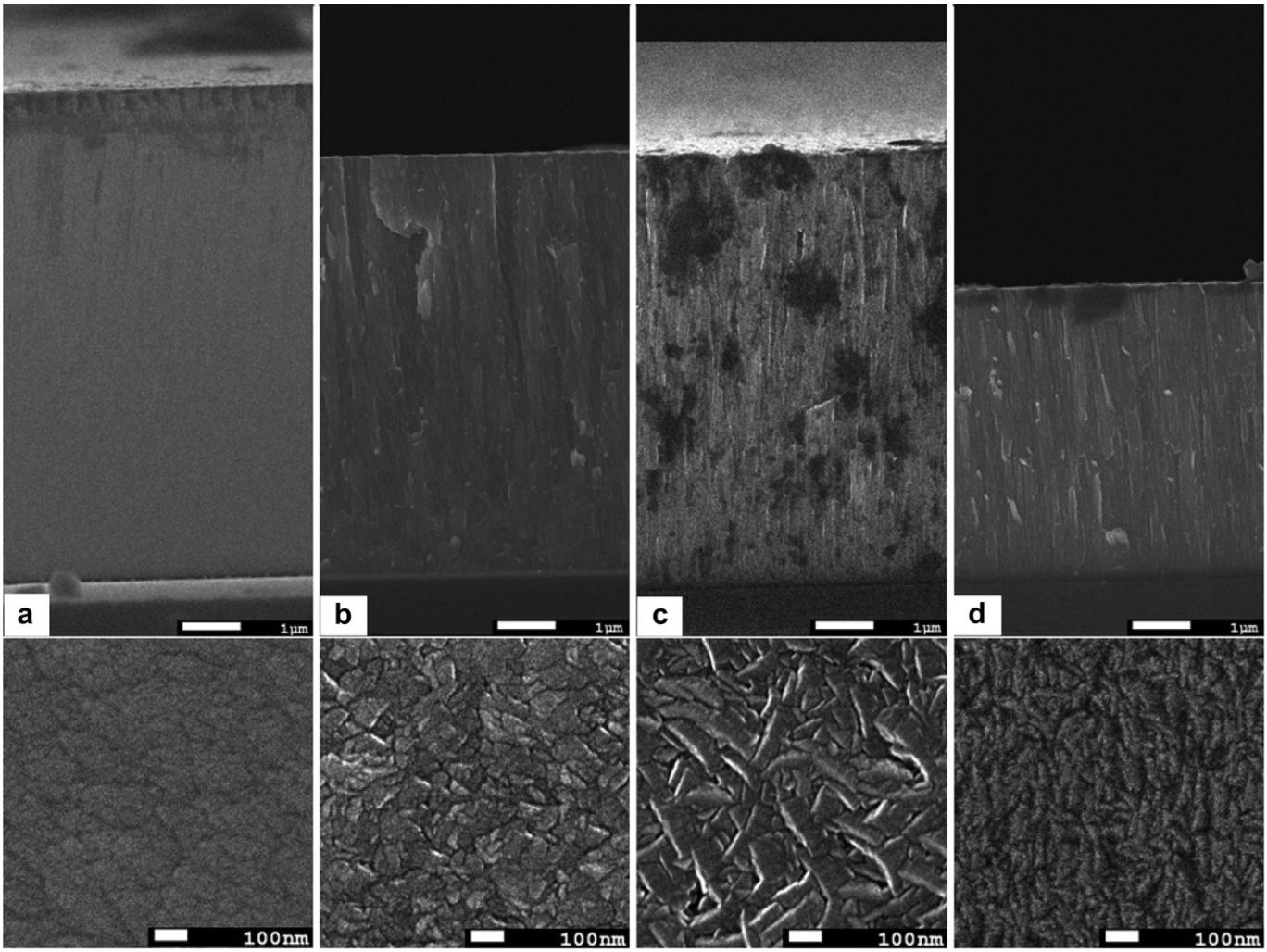

Fig. 4. Secondary electron images of the cross-sections (top row) and surface (bottom row) of WC–Al–N coatings with Al:W targeted ratios of (a) 1:1, (b) 2:1, (c) 3:1, and (d) 4:1.

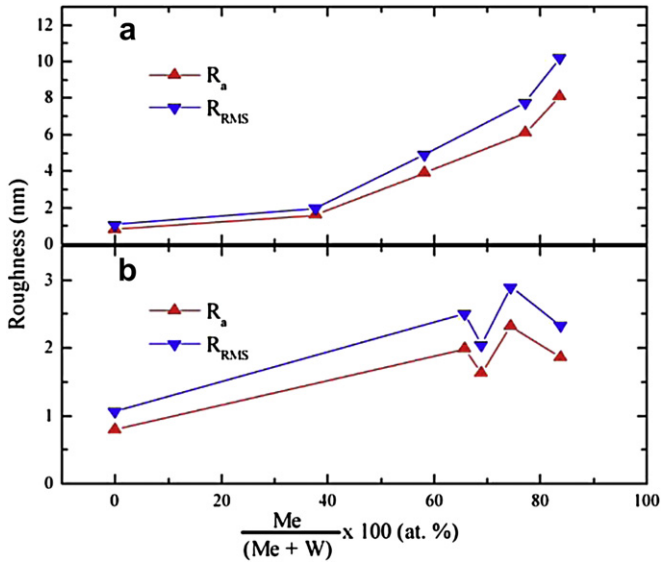

Fig. 5. Surface roughness parameters Ra and RMS as functions of the measured (a) Cr and (b) Al content (at.%). The data for WC_{1-x} binary coating are given as a reference.

284.3 eV) as in WC–Cr–N (Fig. 6). The intensity of C1s peaks in the coatings with higher Al:W ratios was too low for reliable determination of their position. Similar phase composition as the WC–Cr–N was suggested for the WC–Al–N coatings, with AlN replacing CrN. Interestingly, in spite of the presence of a few at.% of oxygen in the coatings, the W–O bonding was not observed in the XPS spectra of WC–Cr–N and WC–Al–N coatings. This means a partial oxidation of primarily CrN and AlN components of the coatings, although the Cr2p and Al2p energy levels are only broadened without noticeable splitting. While the use of an 80/20

Table 2
Cr:W and Al:W ratios and the elemental composition of WC–Cr–N and WC–Al–N coatings, as measured by EDS.

System	Targeted ratio, Me:W	Actual ratio, Me:W	Composition, at.%				
			Al, Cr	W	C	N	O
WC–Cr–N	1:1	0.6:1	11.9	19.7	14.4	53.3	0.7
WC–Cr–N	2:1	1.39:1	23.1	16.6	14.4	38.7	7.3
WC–Cr–N	3:1	3.37:1	32	9.5	9.9	42.3	6.3
WC–Cr–N	4:1	5.13:1	34.9	6.8	9.6	41.4	7.5
WC–Al–N	1:1	2.21:1	29.7	13.4	13.1	38.4	5.4
WC–Al–N	2:1	2.89:1	32.4	11.2	6.6	43.9	5.9
WC–Al–N	3:1	5.13:1	34.4	6.7	3.5	41.8	13.6
WC–Al–N	4:1	10.14:1	36.5	3.6	2.3	38.6	19

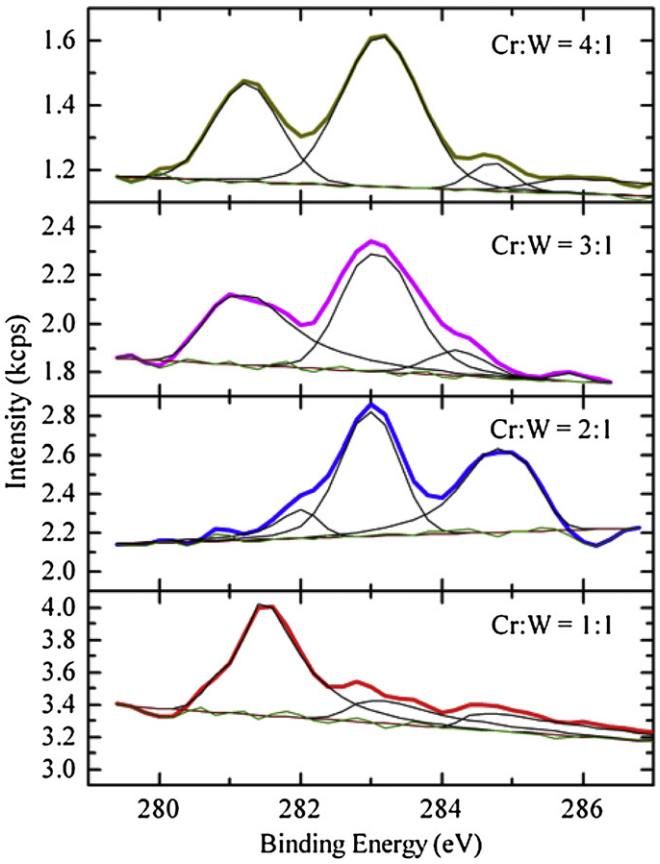

Fig. 6. XPS spectra of C1s core electron energy level and its fittings in WC–Cr–N coatings with different compositions.

Ar/N_2 gas mixture was necessary for plasma stability, this choice resulted in a lower partial pressure of N_2 during the process and, consequently, lower nitrogen content in the coatings (Table 2) [36,37]. Therefore, excess Al may be available for oxidation upon exposure to air after the extraction from the vacuum chamber. This hypothesis is partially supported by the EDS data. Increased oxygen content matches very well with increased Al content. There is no clear oxidation trend in the data for WC–Cr–N coatings.

4. Conclusions

Nanocrystalline quaternary WC–Cr–N and WC–Al–N coatings with thickness in the range of 3.5 μm–8.2 μm and various compositions were successfully deposited on silicon substrates by reactive RF-magnetron sputtering in Ar/N_2 gas mixture using tungsten carbide and Cr or Al targets.

There is a clear relationship found between the deposition conditions and the resulting film structure, composition, and surface morphology. WC–Cr–N and WC–Al–N coatings with the amount of tungsten of more than 50 at.% of total metal content demonstrated dense nearly featureless microstructure, and the coatings with lower tungsten content form columnar grain microstructure with different surface morphologies depending on the process parameters.

It has been proposed that crystalline tungsten carbide (with partial N-substitution of C atoms) and chromium (or aluminum) nitride phases coexist in the coatings with the Cr (or Al):W ratios of 1:1 or less (amount of tungsten of more than 50 at.% of total metal content), while at higher Cr (or Al):W ratios (lower tungsten content) the dominating crystalline phase is either W-doped CrN_{1-y} or AlN_{1-y} solid solution, with WC_{1-x} and small amounts of free sp^2-bonded carbon present as X-ray amorphous phases.

The examination of physical and chemical properties of these quaternary coatings and high-resolution electron microscopy studies for detailed characterization of their structure are the next natural steps in the evaluation of the prospects of such materials.

Acknowledgements

The work in this study has been supported by the U.S. National Science Foundation under the awards DMR-0806521, DRM-0922910, and Regional Council of Burgundy, France.

References

[1] Veprek S, Veprek-Heijman MJG. Surf Coat Technol 2008;202:5063.
[2] Hovsepian PE, Munz WD. In: Cavaliero A, DeHousson JThM, editors. Nanostructured coatings. NY: Springer; 2006. p. 555–644.
[3] Musil J. Surf Coat Technol 2000;125:322.
[4] Raveh A, Zukerman I, Shneck R, Avni R, Fried I. Surf Coat Technol 2007;201:6136.
[5] Karimi A, Wang Y, Cselle T, Morstein M. Thin Solid Films 2002;420–421:275.
[6] Kamiya S, Amaki S, Hanyu H, Yamanobe K, Saka M. Surf Coat Technol 2005;200:876.
[7] Houska J, Vlcek J, Potocky S, Perina V. Diam Relat Mater 2007;16:29.
[8] Guo Y, Ma S, Xu K. Surf Coat Technol 2007;201:5240.
[9] Musil J, Hruby H. Thin Solid Films 2000;365:104.
[10] Abraham S, Ok JT, Kim KH. J Mater Proc Technol 2007;187–188:571.
[11] Stanishevsky A, Lappalainen R. Surf Coat Technol 2000;123:101.
[12] Ma SL, Ma DY, Guo Y, Xu B, Wu GZ, Xu KW, et al. Acta Materialia 2007;55:6350.
[13] Yun JH, Heo SJ, Kim KR, Kim KH. J Vac Sci Technol A 2008;26:146.
[14] Yau BS, Chu CW, Lin D, Lee W, Duh JG, Lin CH. Thin Solid Films 2008;516:1877.
[15] Su YL, Su CT, Yao SH, Yur JP, Hsu CA, Liu TH. Vacuum 2006;80:1021.
[16] Li Y, Gao Y, Xiao B, Min T, Fan Z, Ma S, et al. J Alloys Compounds 2010;502:28.
[17] Warren A, Nylund A, Olefjord I. Int J Refract Metals Hard Mater 1996;14:345.
[18] Suetin GD, Shein IR, Ivanovskii AL. Rus J Inorg Chem 2009;54:1433.
[19] Yan J, Ma X, Zhao W, Tang H, Zhu C, Cai S. Mater Sci Eng B 2005;117:321.
[20] Wu FB, Tien SK, Duh JG, Lee JW. J Electron Mater 2005;34:1533.
[21] Hones P, Diserens M, Sanjines R, Levy F. J Vac Sci Technol B 2000;18:2851.
[22] Lin CH, Duh JD, Yau BS. Surf Coat Technol 2006;201:1316.
[23] Weil KS. J Solid State Chem 2004;177:1976.
[24] Principe EL, Shaw BA. Corrosion 1997;53:675.
[25] Hones P, Consiglio R, Randall N, Levy F. Surf Coat Technol 2000;125:179.
[26] Wu FB, Tien SK, Duh JG. Surf Coat Technol 2005;200:1514.
[27] Toby BH. J Appl Crystallogr 2005;38:1040.
[28] ICDD. In: Kabekkodu S, editor. Powder diffraction file; 2007.
[29] Cheng H, Sun Y, Hing P. Thin Solid Films 2003;434:112.
[30] Ohuchi FS, Russell PE. J Vac Sci Technol A 1987;5:1630.
[31] Zou W, PhD thesis. Charlottesville, VA: University of Virginia; 2001.
[32] Gerbig YB, Spassov V, Savan A, Chetwynd DG. Thin Solid Films 2007;515:2903.
[33] Alami J, Sarakinos K, Uslu F, Wuttig M. J Phys D 2009;42:015304.
[34] Rahmati A. Vacuum 2011;85:853.
[35] Brieseck M, Bohn M, Lengauer W. J Alloys Compounds 2010;489:408.
[36] Koskinen J, Torri P, Hirvonen JP, Mahiout A, Stanishevsky A. Surf Coat Technol 1996;80:57.
[37] Borges J, Vaz F, Marques L. Appl Surf Sci 2010;257:1478–83.